



## 1 **Impact of low-pressure systems on winter heavy air pollution in the northwest Sichuan Basin, China**

2 Guicai Ning<sup>1</sup>, Shigong Wang<sup>2,1</sup>, Steve Hung Lam Yim<sup>3,4</sup>, Jixiang Li<sup>1</sup>, Yuling Hu<sup>1</sup>, Ziwei Shang<sup>1</sup>, Jinyan Wang<sup>1</sup>, Jiaxin  
3 Wang<sup>2</sup>

4 <sup>1</sup>The Gansu Key Laboratory of Arid Climate Change and Reducing Disaster, College of Atmospheric Sciences,  
5 Lanzhou University, Lanzhou 730000, China

6 <sup>2</sup>Key Laboratory of Education Bureau of Sichuan Province for Mountain Environmental Meteorology and Public  
7 Health, School of Atmospheric Sciences, Chengdu University of Information Technology, Chengdu 610225, China

8 <sup>3</sup>Department of Geography and Resource Management, The Chinese University of Hong Kong, Hong Kong, China

9 <sup>4</sup>The Institute of Environment, Energy and Sustainability, The Chinese University of Hong Kong, Hong Kong, China

10 Correspondence to: Shigong Wang ([wangsg@cuit.edu.cn](mailto:wangsg@cuit.edu.cn), [wangsg@lzu.edu.cn](mailto:wangsg@lzu.edu.cn))

### 11 **Abstract**

12 The cities of Chengdu, Deyang, and Mianyang in the northwest Sichuan Basin are part of a rapidly developing  
13 urban agglomeration adjoining the eastern slopes of the Tibetan Plateau. Heavy air pollution events have frequently  
14 occurred over the cities in recent decade, but the effects of meteorological conditions on these pollution events are  
15 unclear. We explored the effects of weather systems on winter heavy air pollution from 1 January 2006 to 31 December  
16 2012 and from 1 January 2014 to 28 February 2017. Ten heavy air pollution events occurred during the research period  
17 and eight of these took place while the region was affected by a dry low-pressure system at 700 hPa. When the urban  
18 agglomeration was in front of the low-pressure system and the weather conditions were controlled by a warm southerly  
19 air flow, and a strong temperature inversion appeared above the atmospheric boundary layer acting as a lid. Forced by  
20 this strong inversion layer, the local secondary circulation was confined within the atmospheric boundary layer and the  
21 horizontal wind speed in the lower troposphere was low. As a result, vertical mixing and horizontal dispersion in the  
22 atmosphere were poor, favoring the formation of heavy air pollution events. After the low-pressure system had  
23 transited over the region, the weather conditions in the urban agglomeration were controlled by a dry and cold air flow  
24 from the northwest at 700 hPa. The strong inversion layer gradually dissipated, the secondary circulation enhanced and  
25 uplifted, and the horizontal wind speed in the lower troposphere also increased, resulting in a sharp decrease in the



26 concentration of air pollutants. The strong inversion layer above the atmospheric boundary layer induced by the  
27 low-pressure system at 700 hPa thus played a key role in the formation of heavy air pollution during the winter months  
28 in this urban agglomeration. This study provides scientific insights for forecasting heavy air pollution in this region of  
29 China.

## 30 **1 Introduction**

31 Air quality, especially the occurrence of heavy air pollution events, is not only strongly affected by excessive  
32 emission of air pollutants, but is also closely associated with meteorological conditions, including atmospheric  
33 circulations, weather systems, structures of atmospheric boundary layer, and the corresponding meteorological  
34 parameters (Ye et al., 2016;Zhang et al., 2012a;Wei et al., 2011;Deng et al., 2014;Li et al., 2015;Gu and Yim, 2016).  
35 The total amount of pollutants emitted in a particular period of time is usually stable in China (Wu et al., 2017), but  
36 there are large differences in the concentrations of air pollutants, indicating that the meteorological conditions have an  
37 important role in modulating concentrations of ambient air pollutants (Wang et al., 2009;Wang et al., 2010;Yang et al.,  
38 2011;Gao et al., 2011;Ji et al., 2012;Hu et al., 2014;Ji et al., 2014).

39 Weather systems control the ability of the atmosphere to disperse pollutants and thus provide the primary driving  
40 force for variations in regional air pollution (Ye et al., 2016;Chen et al., 2008). Leśniok et al. (2010) reported that the  
41 atmosphere was stagnant and that the concentrations of near-ground air pollutants increased significantly in Upper  
42 Silesia, Poland during periods with an anticyclonic circulation. By contrast, when a cyclonic circulation prevailed,  
43 causing an inflow of fresh air masses from regions with lower levels of pollution, the concentrations of air pollutants  
44 decreased. As synoptic-scale high-pressure ridges at 500 hPa transit across Utah, accompanied by warm advection  
45 above valleys, the stability of the atmosphere is increased and favors the formation of persistent pools of cold air,  
46 resulting in deterioration in air quality (Whiteman et al., 2014).

47 Many studies have been carried out on the impact of weather systems on air quality in China. Bei et al. (2016)  
48 classified typical synoptic situations and evaluated their contributions to air quality in the Guanzhong Basin, China.



49 They found that an inland high-pressure system at 850 hPa resulted in temperature inversion, low horizontal wind  
50 speed and a shallow atmospheric boundary layer, which favor the formation of heavy air pollution. Weather systems  
51 have significantly impact on the transport of air pollutants. Luo et al. (2018) reported that the trans-boundary air  
52 pollution and the pollutant concentration in Hong Kong increased when a tropical cyclones is approaching. During  
53 winter, floating dust particles over northwestern China can be carried downstream to northern China by the prevailing  
54 northwesterly winds at 700 hPa, where they mix with anthropogenic pollution to form a regional haze (Tao et al.,  
55 2014;Tao et al., 2012). Changes in weather systems also significantly influence air quality. Shallowing of the East  
56 Asian trough and weakening of the Siberian high-pressure in winter can induce weak horizontal advection and vertical  
57 convection in the lower troposphere, reducing the height of the boundary layer in the Beijing–Tianjin–Hebei region  
58 and favoring the formation of haze (Zhang et al., 2016).

59 The deep Sichuan Basin to the east of the Tibetan Plateau has a maximum elevation difference >2000 m, and is  
60 ranked fourth in China for heavy air pollution after the Beijing–Tianjin–Hebei region, the Yangtze River Delta, and the  
61 Pearl River Delta (Zhang et al., 2012b;Tian et al., 2017). The complex terrain leads to unique weather systems that  
62 affect air quality in this region (Chen et al., 2014;Huang et al., 2017). Low-pressure systems, such as a southwest  
63 vortex and low trough, are often formed at 700 hPa due to the dynamic and thermodynamic effects of the Tibetan  
64 Plateau (Wang and Tan, 2014;Yu et al., 2016) and have different characteristics in different seasons. They are warm  
65 and moist low-pressure systems in summer and autumn and have crucial effects on local precipitation (Peng and  
66 Cheng, 1992;Feng et al., 2016); much work has been carried out in an attempt to understand the impacts of these  
67 low-pressure systems on precipitation (Kuo et al., 1988;Kuo et al., 1986;Chen et al., 2015;Ni et al., 2017;Fu et al.,  
68 2011). In winter and spring, however, these low-pressure systems are both dry and cold (Feng et al., 2016). No attempt  
69 has previously been made to investigate the association between air quality and these dry and cold low-pressure  
70 systems.

71 Chengdu, Deyang, and Mianyang, have undergone rapid development to form an urban agglomeration in the



72 northwest Sichuan Basin. This urban agglomeration lies close to the eastern slopes of Tibetan Plateau, and is affected  
73 by low-pressure systems moving east from the plateau (Feng et al., 2016). Heavy air pollution events have frequently  
74 occurred over there in recent decade. Number of days with exceedance of Grade II standards (MEP, 2012) is more than  
75 150 days each year in Chengdu (Ning et al., 2018). Most previous studies have investigated the basic characteristics of  
76 air pollution (Luo et al., 2001;Chen and Xie, 2012;Tao et al., 2013a;Tao et al., 2013b;Chen et al., 2014;Zhang et al.,  
77 2017;Ning et al., 2018) and the related meteorological parameters (Li et al., 2015;He et al., 2017;Liao et al., 2017;Zeng  
78 and Zhang, 2017). However, the influencing mechanism of dry low-pressure system on heavy air pollution events has  
79 yet to be comprehensively explored. The main purpose of this study was to statistically analyze the relationships  
80 between low-pressure systems and winter heavy air pollution events in this urban agglomeration, and to explore the  
81 physical mechanisms involved in the formation of winter heavy air pollution. This study can deepen our understanding  
82 of the meteorological causes of heavy air pollution events in winter, and provide scientific insights that can be used by  
83 local governments to take effective measures to mitigate air pollution.

84 This paper is organized as follows. The data and methods are described in Section 2. Section 3 provides a  
85 statistical analysis of the relationships between the low-pressure systems and winter heavy air pollution. Section 4  
86 illustrates the physical mechanisms of the effect of weather systems on air pollution and our conclusions are  
87 summarized in Section 5.

## 88 **2 Data and methods**

### 89 **2.1 Air quality data**

90 Air pollution in the Sichuan Basin during the winter months is mainly caused by particulate matter (Ning et al.,  
91 2018). The Chinese Ministry of Environmental Protection (MEP) currently monitors particles with diameters  $\leq 2.5 \mu\text{m}$   
92 ( $\text{PM}_{2.5}$ ) and particles with diameters  $\leq 10 \mu\text{m}$  ( $\text{PM}_{10}$ ). We studied heavy air pollution events occurring during the winter  
93 months in Chengdu, Deyang, and Mianyang in the northwest Sichuan Basin (**Fig. 1**). We selected pollution events with  
94 a daily  $\text{PM}_{10}$  mean concentration  $\geq 350 \mu\text{g m}^{-3}$  from 1 January 2006 to 31 December 2012 and from 1 January 2014 to



95 28 February 2017. The third revision of the “Ambient Air Quality Standard” (AAQS) (GB3095-12) was released on  
96 February 29<sup>th</sup>, 2012, and PM<sub>2.5</sub> was adopted into the AAQS in China since 2013. The air quality monitoring stations  
97 needed to be updated and the data of air pollutants monitored in the three cities existed missing measurement during  
98 2013. Thus, the winter heavy pollution events during 2013 had not been analyzed in this paper. The PM<sub>10</sub> daily mean  
99 concentration from 1 January 2006 to 31 December 2012 refers to the 24-hour average concentration of PM<sub>10</sub> from  
100 12:00 BST (Beijing Standard Time, i.e., Coordinate Universal Time (UTC) +8 h) on the previous day to 12:00 BST on  
101 the current day. The PM<sub>10</sub> daily mean concentration from 1 January 2014 to 28 February 2017 refers to the 24-hour  
102 average concentration of PM<sub>10</sub> from 00:00 BST to 24:00 BST on the current day. Hourly concentrations of PM<sub>2.5</sub>,  
103 sulfur dioxide (SO<sub>2</sub>), nitrogen dioxide (NO<sub>2</sub>), carbon monoxide (CO), and ozone (O<sub>3</sub>) were also measured in the three  
104 cities from 1 January 2014 to 28 February 2017. These above air quality data were collected from the MEP website  
105 (<http://datacenter.mep.gov.cn/index>).

## 106 2.2 Meteorological data

### 107 (1) ERA-Interim daily data

108 To analyze the weather systems at 700 hPa, and the dynamic and thermodynamic conditions in the lower  
109 troposphere, the temperature, the geopotential, the vertical velocity, and the u and v components of wind during the  
110 study period were obtained from the ERA-Interim daily dataset (0.125° × 0.125° grids) from 950 to 500 hPa for a total  
111 of 14 vertical layers (with a vertical separation of 25 hPa from 950 to 775 hPa and a vertical separation of 50 hPa from  
112 750 to 500 hPa). These meteorological data are available for 00:00, 06:00, 12:00, and 18:00 UTC and were collected  
113 from the website (<http://apps.ecmwf.int/datasets/data/interim-full-daily/levtype=pl/>). The height of the atmospheric  
114 boundary layer was obtained from the ERA-Interim daily dataset at the surface with a 3 h temporal resolution (00:00,  
115 03:00, 06:00, 09:00, 12:00, 15:00, 18:00, and 21:00 UTC)  
116 (<http://apps.ecmwf.int/datasets/data/interim-full-daily/levtype=sfc/>) to explore the structure of the atmospheric  
117 boundary layer.



## 118 (2) Sounding data

119 Radiosonde measurements from launches at Wenjiang station (see **Fig. 1**) in Chengdu city (30.70 °N, 103.83 °E,  
120 elevation 541.0 m) at 08:00 and 20:00 BST were obtained from the University of Wyoming website  
121 (<http://weather.uwyo.edu/upperair/sounding.html>) and included the temperature, potential temperature, and horizontal  
122 wind. These data were used to investigate the dynamic and thermodynamic structure of the lower troposphere.

## 123 (3) Visibility

124 Visibility from three observation stations in the three cities was provided by the National Meteorological  
125 Information Center of the China Meteorological Administration, and was also used in this paper.

## 126 2.3 Quantitative measures of meteorological conditions

### 127 2.3.1 Lower tropospheric stability

128 The lower tropospheric stability (LTS) is defined as the difference in the potential temperature between 700 hPa  
129 and the surface (Slingo, 1987), and can be used to describe the thermodynamic state of the lower troposphere (Guo et  
130 al., 2016a; Guo et al., 2016b). The LTS can be used to quantitatively evaluate the vertical mixing of air pollutants in the  
131 lower troposphere:

$$132 \text{ LTS} = \theta_{700\text{hPa}} - \theta_{\text{surface}} \quad (1)$$

133 A large LTS represents a high degree of stability in the lower troposphere and indicates the potential for the weak  
134 vertical mixing of air pollutants.

### 135 2.3.2 The mean wind speed in the lower troposphere

136 To quantitatively evaluate the horizontal dispersion of air pollutants, the mean wind speed (MWS) in the lower  
137 troposphere was defined as:

$$138 \text{ MWS} = \frac{1}{h} \int_0^h \bar{V}(z) dz \quad (2)$$

139 where  $h$  is the height above the ground at 700 hPa and  $\bar{V}(z)$  is the wind speed in the lower troposphere. This can be



140 simplified as follows:

$$141 \quad MWS = \frac{1}{h} \sum_{i=1}^n \left[ \overline{V}_i(z_i) + \overline{V}_{i-1}(z_{i-1}) \right] \cdot 0.5 \cdot \Delta z_i \quad (3)$$

142 where  $n$  is the number of vertical layers from the ground to 700 hPa isobaric layer (including the 700 hPa isobaric  
143 layer),  $\overline{V}_i(z_i)$  is the wind speed in a vertical layer (when  $i=0$  represents the wind speed on the ground and  $i=n$   
144 represents the wind speed at 700 hPa), and  $\Delta z_i$  is the difference in height between the two adjacent vertical layers. A  
145 large value of MWS suggests strong horizontal dispersion of air pollutants.

### 146 **3 Heavy air pollution events and weather conditions**

#### 147 **3.1 Overview of the heavy air pollution events**

148 A total of ten heavy winter air pollution events occurred from 1 January 2006 to 31 December 2012 and from 1  
149 January 2014 to 28 February 2017 in the urban agglomeration of Chengdu, Deyang, and Mianyang. Nine events were  
150 accompanied by a low-pressure system at 700 hPa, and the low-pressure systems in eight events were dry and didn't  
151 induce precipitation. This paper explores the impacts of dry low-pressure systems on the eight winter heavy air  
152 pollution events (see **Table 1** for a summary of these eight events).

153 **Table 1** shows that there was low visibility during these eight heavy air pollution events in which particulate  
154 matter is the primary pollutants. Six of the eight events were classified as persistent air pollution events, which are  
155 harmful to the health of local residents (Chow et al., 2006;Langrish et al., 2012;Lim et al., 2012;Guo et al., 2016c), and  
156 the longest duration was 10 days. Most of the heavy air pollution events had the characteristics of regional pollution,  
157 with five pollution events occurring in multiple cities. Two heavy air pollution events (events 6 and 7) occurred during  
158 the Spring Festival, with maximum daily mean  $PM_{10}$  concentrations up to 403 and 562  $\mu g m^{-3}$  on the Chinese New  
159 Year Day. This suggests that the centralized letting off of fireworks during the traditional Chinese Spring Festival,  
160 accompanied by poor conditions for the dispersion of air pollution, may lead to a sharp increase in the concentration of  
161 particulate pollutants near ground level within a short period of time (Liao et al., 2017;Wang et al., 2007;Shi et al.,



162 2011;Huang et al., 2012).

### 163 **3.2 Weather systems and meteorological conditions during heavy air pollution events**

164 An analysis of the synoptic conditions showed that the urban agglomeration was affected by low-pressure systems  
165 (low vortex or low trough) at 700 hPa during periods of deteriorating air quality in the eight heavy air pollution events  
166 (**Fig. 2**). These studied areas were all located in front of low-pressure systems and were controlled by a southerly warm  
167 air flow (**Fig. 2**). Weather systems can be characterized by their relative vorticity. A positive relative vorticity usually  
168 corresponds to a low-pressure system, whereas a negative relative vorticity usually represents a high-pressure system.  
169 Thus the relative vorticity at 700 hPa was analyzed during periods of both deteriorating and improving air quality  
170 (**Table 2**).

171 **Table 2** shows that the relative vorticities at 700 hPa during periods of deteriorating air quality were all positive.  
172 This indicated that the study areas were located in front of low-pressure systems at 700 hPa. As a result, a southerly  
173 warm air flow dominated at 700 hPa and led to an increase in temperature above the atmospheric boundary layer,  
174 which increased atmospheric stability and favored the formation of an air pollution event. During periods of improving  
175 air quality, the relative vorticities at 700 hPa of six heavy air pollution events (except for events 6 and 7) were negative,  
176 showing that the low-pressure systems had transited across the study areas. These areas were thus controlled by a  
177 northerly dry, cold air flow at 700 hPa. As a consequence, the temperature above the atmospheric boundary layer  
178 decreased and the stability of the atmosphere weakened, which favored the vertical mixing of air pollutants.

179 To explore the impacts of low-pressure systems on the structure of the atmospheric boundary layer, the boundary  
180 layer height during periods of deteriorating and improving air quality were analyzed for each heavy air pollution event  
181 (**Table 3**). In most of the heavy air pollution events, the height of the boundary layer increased after the low-pressure  
182 system had passed across the study area. However, the increase in the height of the boundary layer was not as  
183 significant as that seen in Eastern China (Ji et al., 2012;Quan et al., 2013;He et al., 2015;Leng et al., 2016;Qu et al.,  
184 2017) and the boundary layer heights in air pollution events 3, 4, and 6 decreased after transit of the low-pressure



185 system. These results show that the effects of the transit of low-pressure systems at 700 hPa on the height of the  
186 boundary layer were weak. It is therefore difficult to explain the variations in the concentrations of air pollutants in the  
187 study areas by considering only the meteorological conditions within the boundary layer.

188 Previous studies have shown that the meteorological conditions above the boundary layer should also be  
189 considered (Slingo, 1987;Guo et al., 2016a;Guo et al., 2016b). Therefore an index of the MWS in the lower  
190 troposphere was proposed and this index, together with the LTS of the eight heavy air pollution events, was further  
191 investigated (**Table 3**). The differences in the potential temperature between 700 hPa and the surface during periods of  
192 deteriorating air quality in the eight events were all  $\geq 18.54$  K and the maximum value was 29.45 K, indicating that the  
193 lower troposphere was very stable. The MWS was  $\leq 4.22$  m s<sup>-1</sup> for all eight events, with a minimum of 1.91 m s<sup>-1</sup>.  
194 These results show that the low-pressure systems resulted in the stagnation of air in the lower troposphere. After the  
195 low-pressure systems had transited the study area, the lower tropospheric stability significantly decreased, with a  
196 maximum decrease in the LTS of up to -11.23 K, and the MWS increased. This showed that the arrival of a dry, cold  
197 air flow induced by the transit of the low-pressure system significantly weakened the stability of the lower troposphere  
198 and increased the wind speed, improving air quality.

199 In events 6 and 7, however, although the study areas were still located in front of the low-pressure system and the  
200 capacity for dispersion had not yet improved, the concentrations of particulate matter began to sharply decrease before  
201 the transit of the low-pressure system. Both of these events occurred during the Chinese Spring Festival. After the  
202 Chinese New Year Day, the letting off of fireworks stopped and the emission of air pollutants was significantly  
203 reduced, resulting in a sharp decrease in the concentration of particulate matter (Wang et al., 2007;Shi et al., 2011;Liao  
204 et al., 2017). The decrease in the magnitude of the daily mean concentration of PM<sub>10</sub> in event 7 was up to 350  $\mu\text{g m}^{-3}$ .  
205 These eight heavy air pollution events in the northwest Sichuan Basin can therefore be categorized into two types  
206 based on their date of occurrence. The two heavy air pollution events (6 and 7) occurring during the Chinese Spring  
207 Festival were categorized as Spring Festival excessive emission heavy air pollution events. The other six events



208 (events 1–5 and 8) were categorized as normal heavy air pollution events.

#### 209 **4 Impacts of low-pressure systems on heavy air pollution events**

210 To further explore the mechanism involved in the formation of heavy air pollution events, with a particular  
211 emphasis on the effect of low-pressure systems on air quality, a typical event was selected from the eight events  
212 described in the preceding section. The variations in air quality and the dynamic and thermodynamic conditions in the  
213 lower troposphere of the selected event were analyzed. Additionally, the impacts of Spring Festival excessive emission  
214 on heavy air pollution events also been investigated.

##### 215 **4.1 The influencing mechanism of low-pressure systems on heavy air pollution events**

216 Heavy air pollution event 8 occurred from 1 January 2017 to 6 January 2017 (Table 3) and the most polluted area  
217 was Chengdu. The maximum daily mean concentrations of PM<sub>2.5</sub> and PM<sub>10</sub> occurred on 5 January 2017. The  
218 maximum PM<sub>10</sub> daily mean concentration in Chengdu was up to 480 µg m<sup>-3</sup>. The concentrations of particulate matter  
219 increased sharply (**Fig. 3**) from 00:00 BST on 3 January 2017 to 00:00 BST on 5 January 2017 and the concentrations  
220 of nitrogen dioxide and carbon monoxide also showed an increasing trend. Since 12:00 BST on 5 January 2017, the  
221 concentrations of particulate matter decreased significantly (**Fig. 3**).

222 **Fig. 4** shows the weather maps at 700 hPa during event 8. **Fig. 4a** shows that there was no low-pressure system at  
223 700 hPa over the urban agglomeration at 02:00 BST on 2 January and there was a dry, cold air flow from the northwest.  
224 A low trough was generated at 700 hPa on the west side of the urban agglomeration at 14:00 BST on 2 January 2017.  
225 This trough later developed and was enhanced, the urban agglomeration was still located at the front of the trough and  
226 was controlled by a warm, moist air flow from the southwest until 02:00 BST on 5 January 2017 (**Fig. 4b** and **4c**). The  
227 concentrations of particulate matter in the urban agglomeration increased sharply and the air quality deteriorated. The  
228 trough developed further and a low vortex was formed, which transited across over the study area at 02:00 BST on 5  
229 January 2017 (**Fig. 4d**). The urban agglomeration was then located behind the low vortex and was controlled by a  
230 northerly dry, cold air flow (**Fig. 4d**) and the air pollutants were rapidly dispersed.



231 The west–east vertical cross-sections of the 24-hour change in temperature and wind vectors (u and w) in the most  
232 polluted area (30.75 ° N) (**Fig. 5**) and the vertical profiles of temperature and horizontal wind speed (**Fig. 6**) were  
233 analyzed to investigate the effects of the low-pressure system on the dynamic and thermodynamic dispersion of air  
234 pollutants in the lower troposphere.

235 **Fig.4b** and **4c** shows that the urban agglomeration was located in front of the low-pressure system and was  
236 controlled by a southerly warm air flow. There was a descending motion between the top of the boundary layer and  
237 500 hPa (**Fig. 5a** and **5b**). Under the effects of warm advection and descending motion, a warming center appeared  
238 between 800 and 650 hPa (**Fig. 5a–c**) and the maximum increase in the 24-hour temperature was up to 10 °C (**Fig. 6a**).  
239 Weak cooling occurred below 800 hPa, a strong temperature inversion appeared between 775 and 650 hPa (**Fig. 6a**),  
240 and the stability of the lower troposphere increased. The urban agglomeration was dominated by the low-pressure  
241 system for a long time and a long-lasting strong temperature inversion was therefore induced and maintained above the  
242 boundary layer. This was different from the temperature inversion that is often seen within the boundary layer in  
243 Eastern China (Ji et al., 2012;Li et al., 2012;Wang et al., 2014;Li and Chan, 2016;Zhang and Niu, 2016). The  
244 temperature inversion acted as a lid over the boundary layer, suppressing the dispersion of air pollutants. This lid effect  
245 restrained vertical mixing in the atmosphere and the local secondary circulation was therefore confined in the boundary  
246 layer, with its center located at about 850 hPa (**Fig. 5a–c**). The horizontal wind speed below 800 hPa was  $\leq 2 \text{ m s}^{-1}$  (**Fig.**  
247 **6b**). These results indicate that vertical mixing and horizontal dispersion were weak, causing accumulation of air  
248 pollutants at the ground level. The concentrations of particulate matter then sharply increased to their peak value (**Fig.**  
249 **3**), generating a heavy air pollution event.

250 A low vortex and trough at 700 hPa transited across the urban agglomeration and a northwesterly dry, cold air flow  
251 prevailed (**Fig. 4d**). Under the influence of the cold air flow, a cooling center appeared between 800 and 650 hPa (**Fig.**  
252 **5d**), whereas the air temperature increased below 800 hPa (**Fig. 5d**). As a result, the stability in the lower troposphere  
253 was weakened and the strong inversion layer gradually disappeared (**Fig. 6a**). The lid effect above the boundary layer



254 also disappeared, resulting in an increase in the local secondary circulation, the center of which was uplifted to 700  
255 hPa (**Fig. 5d**). The horizontal wind speed below 800 hPa also increased (**Fig. 6b**). The air pollutants were able to  
256 disperse over a larger space and the vertical mixing and horizontal dispersion were significantly improved. The air  
257 quality improved and the heavy air pollution event ended.

258 To verify whether the mechanism involved in the formation of event 8 is used for the others heavy air pollution  
259 events, the vertical profiles of temperature and horizontal wind speed in events 1-7 (**Fig. 7**) were explored during the  
260 periods of both the low-pressure system controlling and transited over this urban agglomeration. Similar to the event 8,  
261 a strong temperature inversion appeared over the study area between 800 and 650 hPa (**Fig. 7a**) when the urban  
262 agglomeration was located in the front of low-pressure system and was controlled by a southerly warm air flow at 700  
263 hPa. Meanwhile, the horizontal wind speed was low below 800 hPa; the wind speed at all levels below 850 hPa was  $\leq 2$   
264  $\text{m s}^{-1}$  (**Fig. 7c**). After the low-pressure system had transited across the urban agglomeration, the strong inversion layer  
265 above the boundary layer gradually disappeared (**Fig. 7b**), and the horizontal wind speed in the lower troposphere  
266 increased (**Fig. 7d**). Therefore, the influencing mechanism of low-pressure system on heavy air pollution events is  
267 common in this urban agglomeration.

#### 268 **4.2 Impacts of Spring Festival excessive emission on heavy air pollution events**

269 **Table 1** shows that events 6 and 7 occurred during the Chinese Spring Festival when the concentration of  
270 particulate matter increased sharply. Low concentrations of gaseous pollutants were found throughout these two events,  
271 however, which may be related to a reduction in production or the shut-down of factories, as well as lower numbers of  
272 vehicles during the week-long Spring Festival (Liao et al., 2017). The centralized letting off of fireworks during the  
273 Chinese Spring Festival played an important part in the sharp increase in the concentrations of particulate matter  
274 (Huang et al., 2012; Liao et al., 2017; Shi et al., 2011; Wang et al., 2007). We investigated the impacts of Spring Festival  
275 excessive emission on event 6 and 7.

276 It's noteworthy that the emission of air pollutants increased sharply during this period of deteriorating air quality



277 for event 6 and 7 due to the centralized letting off of fireworks during the Chinese Spring Festival. What's more, under  
278 the effects of low-pressure system, the strong temperature inversion appeared above the atmospheric boundary layer  
279 (**Fig. 7a**) and the horizontal wind speed was low below 800 hPa (**Fig. 7c**). The combination of excessive emissions  
280 with poor dispersion conditions resulted in the maximum daily concentrations of PM<sub>10</sub> occurring on the Chinese New  
281 Year Day (**Table 1**). The maximum daily mean PM<sub>10</sub> concentration of eight heavy air pollution events occurred in  
282 event 7 and was up to 562 µg m<sup>-3</sup> (**Table 1**). This shows that the excessive emissions during the short Chinese Spring  
283 Festival were able to increase the peak concentrations of particulate matter.

284 Unlike in the normal heavy air pollution events, the concentrations of particulate matter began to decrease sharply  
285 in event 6 and 7 before the low-pressure system transited over the urban agglomeration (**Fig. 8a** and **8b**), when the  
286 strong temperature inversion was still present above the atmospheric boundary layer (**Fig. 10**) and the local secondary  
287 circulation was still confined in the atmospheric boundary layer (**Fig. 9a** and **9b**). This indicated that these events were  
288 strongly dependent on emissions. Thus, the centralized letting off of fireworks in the Chinese Spring Festival  
289 combined with the impacts of low-pressure system were the main causes of these two events in this region of China.

## 290 **5 Conclusions and discussions**

291 We investigated the relationships between low-pressure systems and winter heavy air pollution events in the  
292 urban agglomeration of Chengdu, Deyang, and Mianyang in the northwest Sichuan Basin and explored the influence of  
293 dry and cold low-pressure systems on winter air quality.

294 A total of ten heavy winter air pollution events occurred in the urban agglomeration from 1 January 2006 to 31  
295 December 2012 and from 1 January 2014 to 28 February 2017. The meteorological causes of eight of these air  
296 pollution events were attributed to dry low-pressure systems (trough and low vortex) at 700 hPa. The schematic  
297 diagram in **Fig. 11** shows that a strong temperature inversion appeared above the atmospheric boundary layer because  
298 the urban agglomeration was located in front of low-pressure system at 700 hPa and was controlled by a warm  
299 southerly air flow. This strong inversion layer acted as a lid over the boundary layer and suppressed the dispersion of



300 air pollutants, confining the local secondary circulation within the atmospheric boundary layer. The horizontal wind  
301 speed in the lower troposphere was low. As a result, the space available for the vertical and horizontal dispersion of air  
302 pollutants was small. The concentrations of air pollutants increased to their peak values, resulting in heavy air  
303 pollution events.

304 After the low-pressure system had transited across the urban agglomeration, the strong inversion layer above the  
305 boundary layer gradually disappeared, resulting in an increase and uplift of the secondary circulation and an increase in  
306 the horizontal wind speed in the lower troposphere. The space available for the vertical and horizontal dispersion of air  
307 pollutants increased and the concentrations of air pollutants decreased sharply, ending the heavy air pollution event.  
308 The centralized letting off of fireworks during the Chinese Spring Festival was one of the main causes of the heavy air  
309 pollution events in this region of China.

310 The urban agglomeration studied here, which is flanked by the eastern slopes of the Tibetan Plateau, is sensitive  
311 to low-pressure systems moving east from the plateau (Feng et al., 2016). The complex terrain forms local secondary  
312 circulations, which have a significant impact on air quality (Liu et al., 2009; Chen et al., 2009; Miao et al., 2015). We  
313 found that the intensity and altitude of the local secondary circulations were markedly affected by the low-pressure  
314 system and changes in circulation affected the local air quality. The mechanism of influence of the low-pressure  
315 system on the local secondary circulation requires further elaboration using numerical simulation. The centralized  
316 letting off of fireworks during the Chinese Spring Festival significantly affected the air quality (Shi et al., 2011; Huang  
317 et al., 2012; Wang et al., 2007; Liao et al., 2017), especially during some of the heavy air pollution events in the urban  
318 agglomeration, although the impact of fireworks on air quality was remarkably different depending on the dispersion  
319 conditions (Li et al., 2006). Sensitivity research should therefore be carried out using models coupled with detailed  
320 meteorological and chemical processes to quantitatively examine the impacts of the centralized emission of air  
321 pollutants from the Chinese Spring Festival on local air quality.



322 **Competing interests**

323 The authors declare that they have no conflict of interest.

324 **Acknowledgements**

325 This work was supported by the National Natural Science Foundation of China (91644226, 41575138), the National  
326 Key Research Project of China-Strategy on Black Carbon Reduction and Evaluation of the Health Effects of Climate  
327 Change (2016YFA0602004), the Improvement on Competitiveness in Hiring New Faculties Fund (2013/14) of The  
328 Chinese University of Hong Kong and the Vice-Chancellor's Discretionary Fund of The Chinese University of Hong  
329 Kong (4930744). We would like to thank the following departments for the provided data, the Ministry of  
330 Environmental Protection of the People's Republic of China, the European Centre for Medium-Range Weather  
331 Forecasts, the University of Wyoming and the China Meteorological Administration.

332 **References**

- 333 Bei, N., Li, G., Huang, R. J., Cao, J., Meng, N., Feng, T., Liu, S., Zhang, T., Zhang, Q., and Molina, L. T.: Typical synoptic  
334 situations and their impacts on the wintertime air pollution in the Guanzhong basin, China, *Atmos. Chem. Phys.*, 16,  
335 7373-7387, <https://doi.org/10.5194/acp-16-7373-2016>, 2016.
- 336 Chen, Y., Zhao, C., Zhang, Q., Deng, Z., Huang, M., and Ma, X.: Aircraft study of Mountain Chimney Effect of Beijing,  
337 China, *J. Geophys. Res.*, 114, n/a-n/a, <https://doi.org/10.1029/2008JD010610>, 2009.
- 338 Chen, Y., and Xie, S.: Temporal and spatial visibility trends in the Sichuan Basin, China, 1973 to 2010, *Atmos. Res.*, 112,  
339 25-34, <https://doi.org/10.1016/j.atmosres.2012.04.009>, 2012.
- 340 Chen, Y., Xie, S., Luo, B., and Zhai, C.: Characteristics and origins of carbonaceous aerosol in the Sichuan Basin, China,  
341 *Atmos. Environ.*, 94, 215-223, <https://doi.org/10.1016/j.atmosenv.2014.05.037>, 2014.
- 342 Chen, Y., Li, Y., and Zhao, T.: Cause Analysis on Eastward Movement of Southwest China Vortex and Its Induced Heavy  
343 Rainfall in South China, *Adv Meteorol.*, 2015, 22, <https://doi.org/10.1155/2015/481735>, 2015.
- 344 Chen, Z. H., Cheng, S. Y., Li, J. B., Guo, X. R., Wang, W. H., and Chen, D. S.: Relationship between atmospheric pollution  
345 processes and synoptic pressure patterns in northern China, *Atmos. Environ.*, 42, 6078-6087,  
346 <https://doi.org/10.1016/j.atmosenv.2008.03.043>, 2008.
- 347 Chow, J. C., Watson, J. G., Mauderly, J. L., Costa, D. L., Wyzga, R. E., Vedal, S., Hidy, G. M., Altshuler, S. L., Marrack, D.,  
348 Heuss, J. M., Wolff, G. T., Arden Pope Iii, C., and Dockery, D. W.: Health Effects of Fine Particulate Air Pollution:  
349 Lines that Connect, *J. Air Waste Manage. Assoc.*, 56, 1368-1380, <https://doi.org/10.1080/10473289.2006.10464545>,  
350 2006.
- 351 Deng, T., Wu, D., Deng, X., Tan, H., Li, F., and Liao, B.: A vertical sounding of severe haze process in Guangzhou area, *Sci.*



- 352 China Earth Sci., 57, 2650-2656, 10.1007/s11430-014-4928-y, 2014.
- 353 Feng, X., Liu, C., Fan, G., Liu, X., and Feng, C.: Climatology and Structures of Southwest Vortices in the NCEP Climate  
354 Forecast System Reanalysis, J. Climate., 29, 7675-7701, <https://doi.org/10.1175/jcli-d-15-0813.1>, 2016.
- 355 Fu, S., Sun, J., Zhao, S., and Li, W.: The energy budget of a southwest vortex with heavy rainfall over south China, Adv.  
356 Atmos. Sci., 28, 709-724, <https://doi.org/10.1007/s00376-010-0026-z>, 2011.
- 357 Gao, Y., Liu, X., Zhao, C., and Zhang, M.: Emission controls versus meteorological conditions in determining aerosol  
358 concentrations in Beijing during the 2008 Olympic Games, Atmos. Chem. Phys., 11, 12437-12451,  
359 <https://doi.org/10.5194/acp-11-12437-2011>, 2011.
- 360 Gu, Y., and Yim, S. H. L.: The air quality and health impacts of domestic trans-boundary pollution in various regions of  
361 China, Environ. Int., 97, 117-124, <https://doi.org/10.1016/j.envint.2016.08.004>, 2016.
- 362 Guo, J., Deng, M., Lee, S. S., Wang, F., Li, Z., Zhai, P., Liu, H., Lv, W., Yao, W., and Li, X.: Delaying precipitation and  
363 lightning by air pollution over the Pearl River Delta. Part I: Observational analyses, J. Geophys. Res.-Atmos., 121,  
364 6472-6488, <https://doi.org/10.1002/2015JD023257>, 2016a.
- 365 Guo, J., Miao, Y., Zhang, Y., Liu, H., Li, Z., Zhang, W., He, J., Lou, M., Yan, Y., Bian, L., and Zhai, P.: The climatology of  
366 planetary boundary layer height in China derived from radiosonde and reanalysis data, Atmos. Chem. Phys., 16,  
367 13309-13319, <https://doi.org/10.5194/acp-16-13309-2016>, 2016b.
- 368 Guo, Y., Zeng, H., Zheng, R., Li, S., Barnett, A. G., Zhang, S., Zou, X., Huxley, R., Chen, W., and Williams, G.: The  
369 association between lung cancer incidence and ambient air pollution in China: A spatiotemporal analysis, Environ. Res.,  
370 144, 60-65, <https://doi.org/10.1016/j.envres.2015.11.004>, 2016c.
- 371 He, H., Tie, X., Zhang, Q., Liu, X., Gao, Q., Li, X., and Gao, Y.: Analysis of the causes of heavy aerosol pollution in Beijing,  
372 China: A case study with the WRF-Chem model, Particuology, 20, 32-40, <https://doi.org/10.1016/j.partic.2014.06.004>,  
373 2015.
- 374 He, J., Gong, S., Yu, Y., Yu, L., Wu, L., Mao, H., Song, C., Zhao, S., Liu, H., Li, X., and Li, R.: Air pollution characteristics  
375 and their relation to meteorological conditions during 2014–2015 in major Chinese cities, Environ. Pollut., 223,  
376 484-496, <https://doi.org/10.1016/j.envpol.2017.01.050>, 2017.
- 377 Hu, X.-M., Ma, Z., Lin, W., Zhang, H., Hu, J., Wang, Y., Xu, X., Fuentes, J. D., and Xue, M.: Impact of the Loess Plateau on  
378 the atmospheric boundary layer structure and air quality in the North China Plain: A case study, Sci. Total Environ., 499,  
379 228-237, <https://doi.org/10.1016/j.scitotenv.2014.08.053>, 2014.
- 380 Huang, K., Zhuang, G., Lin, Y., Wang, Q., Fu, J. S., Zhang, R., Li, J., Deng, C., and Fu, Q.: Impact of anthropogenic  
381 emission on air quality over a megacity – revealed from an intensive atmospheric campaign during the Chinese Spring  
382 Festival, Atmos. Chem. Phys., 12, 11631-11645, <https://doi.org/10.5194/acp-12-11631-2012>, 2012.
- 383 Huang, Q., Cai, X., Song, Y., and Zhu, T.: Air stagnation in China (1985–2014): climatological mean features and trends,  
384 Atmos. Chem. Phys., 17, 7793-7805, <https://doi.org/10.5194/acp-17-7793-2017>, 2017.
- 385 Ji, D., Wang, Y., Wang, L., Chen, L., Hu, B., Tang, G., Xin, J., Song, T., Wen, T., Sun, Y., Pan, Y., and Liu, Z.: Analysis of  
386 heavy pollution episodes in selected cities of northern China, Atmos. Environ., 50, 338-348,



- 387 <https://doi.org/10.1016/j.atmosenv.2011.11.053>, 2012.
- 388 Ji, D., Li, L., Wang, Y., Zhang, J., Cheng, M., Sun, Y., Liu, Z., Wang, L., Tang, G., Hu, B., Chao, N., Wen, T., and Miao, H.:  
389 The heaviest particulate air-pollution episodes occurred in northern China in January, 2013: Insights gained from  
390 observation, *Atmos. Environ.*, 92, 546-556, <https://doi.org/10.1016/j.atmosenv.2014.04.048>, 2014.
- 391 Kuo, Y.-H., Cheng, L., and Anthes, R. A.: Mesoscale Analyses of the Sichuan Flood Catastrophe, 11–15 July 1981, *Mon.*  
392 *Wea. Rev.*, 114, 1984-2003, [https://doi.org/10.1175/1520-0493\(1986\)114<1984:maotsf>2.0.co;2](https://doi.org/10.1175/1520-0493(1986)114<1984:maotsf>2.0.co;2), 1986.
- 393 Kuo, Y.-H., Cheng, L., and Bao, J.-W.: Numerical Simulation of the 1981 Sichuan Flood. Part I: Evolution of a Mesoscale  
394 Southwest Vortex, *Mon. Wea. Rev.*, 116, 2481-2504, [https://doi.org/10.1175/1520-0493\(1988\)116<2481:nsotsf>2.0.co;2](https://doi.org/10.1175/1520-0493(1988)116<2481:nsotsf>2.0.co;2),  
395 1988.
- 396 Langrish, J. P., Li, X., Wang, S., Lee, M. M. Y., Barnes, G. D., Miller, M. R., Cassee, F. R., Boon, N. A., Donaldson, K., Li, J.,  
397 Li, L., Mills, N. L., Newby, D. E., and Jiang, L.: Reducing Personal Exposure to Particulate Air Pollution Improves  
398 Cardiovascular Health in Patients with Coronary Heart Disease, *Environ Health Perspect.*, 120, 367-372,  
399 <https://doi.org/10.1289/ehp.1103898>, 2012.
- 400 Leng, C., Duan, J., Xu, C., Zhang, H., Wang, Y., Wang, Y., Li, X., Kong, L., Tao, J., Zhang, R., Cheng, T., Zha, S., and Yu, X.:  
401 Insights into a historic severe haze event in Shanghai: synoptic situation, boundary layer and pollutants, *Atmos. Chem.*  
402 *Phys.*, 16, 9221-9234, <https://doi.org/10.5194/acp-16-9221-2016>, 2016.
- 403 Leśniok, M., Małarzewski, Ł., and Niedźwiedz, T.: Classification of circulation types for Southern Poland with an  
404 application to air pollution concentration in Upper Silesia, *Phys. Chem. Earth Parts A B C.*, 35, 516-522,  
405 <https://doi.org/10.1016/j.pce.2009.11.006>, 2010.
- 406 Li, L., Li, J., Xin, L., Li, H., and Wei, Q.: Analysis of atmospheric air pollution of Beijing City in Spring Festival period,  
407 *China Environ. Sci.*, 26, 537-541 (in Chinese), [http://manu36.magtech.com.cn/Jweb\\_zghjcx/CN/](http://manu36.magtech.com.cn/Jweb_zghjcx/CN/) 2006.
- 408 Li, L., and Chan, P. W.: LIDAR observation and numerical simulation of vortex/wave shedding at the Eastern Runway  
409 Corridor of the Hong Kong International Airport, *Meteorol. Appl.*, 23, 379-388, <https://doi.org/10.1002/met.1562>, 2016.
- 410 Li, Y., Yan, J., and Sui, X.: Tropospheric temperature inversion over central China, *Atmos. Res.*, 116, 105-115,  
411 <https://doi.org/10.1016/j.atmosres.2012.03.009>, 2012.
- 412 Li, Y., Chen, Q., Zhao, H., Wang, L., and Tao, R.: Variations in PM<sub>10</sub>, PM<sub>2.5</sub> and PM<sub>1.0</sub> in an Urban Area of the Sichuan  
413 Basin and Their Relation to Meteorological Factors, *Atmosphere.*, 6, 150, 2015.
- 414 Liao, T., Wang, S., Ai, J., Gui, K., Duan, B., Zhao, Q., Zhang, X., Jiang, W., and Sun, Y.: Heavy pollution episodes, transport  
415 pathways and potential sources of PM<sub>2.5</sub> during the winter of 2013 in Chengdu (China), *Sci. Total Environ.*, 584-585,  
416 1056-1065, <https://doi.org/10.1016/j.scitotenv.2017.01.160>, 2017.
- 417 Lim, S. S., Vos, T., Flaxman, A. D., Danaei, G., Shibuya, K., Adair-Rohani, H., AlMazroa, M. A., Amann, M., Anderson, H.  
418 R., Andrews, K. G., Aryee, M., Atkinson, C., Bacchus, L. J., Bahalim, A. N., Balakrishnan, K., Balmes, J., Barker-Collo,  
419 S., Baxter, A., Bell, M. L., Blore, J. D., Blyth, F., Bonner, C., Borges, G., Bourne, R., Boussinesq, M., Brauer, M.,  
420 Brooks, P., Bruce, N. G., Brunekreef, B., Bryan-Hancock, C., Bucello, C., Buchbinder, R., Bull, F., Burnett, R. T., Byers,  
421 T. E., Calabria, B., Carapetis, J., Carnahan, E., Chafe, Z., Charlson, F., Chen, H., Chen, J. S., Cheng, A. T.-A., Child, J.



- 422 C., Cohen, A., Colson, K. E., Cowie, B. C., Darby, S., Darling, S., Davis, A., Degenhardt, L., Dentener, F., Des Jarlais,  
423 D. C., Devries, K., Dherani, M., Ding, E. L., Dorsey, E. R., Driscoll, T., Edmond, K., Ali, S. E., Engell, R. E., Erwin, P.  
424 J., Fahimi, S., Falder, G., Farzadfar, F., Ferrari, A., Finucane, M. M., Flaxman, S., Fowkes, F. G. R., Freedman, G.,  
425 Freeman, M. K., Gakidou, E., Ghosh, S., Giovannucci, E., Gmel, G., Graham, K., Grainger, R., Grant, B., Gunnell, D.,  
426 Gutierrez, H. R., Hall, W., Hoek, H. W., Hogan, A., Hosgood, H. D., Hoy, D., Hu, H., Hubbell, B. J., Hutchings, S. J.,  
427 Ibeanusi, S. E., Jacklyn, G. L., Jasrasaria, R., Jonas, J. B., Kan, H., Kanis, J. A., Kassebaum, N., Kawakami, N., Khang,  
428 Y.-H., Khatibzadeh, S., Khoo, J.-P., Kok, C., Laden, F., Lalloo, R., Lan, Q., Lathlean, T., Leasher, J. L., Leigh, J., Li, Y.,  
429 Lin, J. K., Lipshultz, S. E., London, S., Lozano, R., Lu, Y., Mak, J., Malekzadeh, R., Mallinger, L., Marcenes, W.,  
430 March, L., Marks, R., Martin, R., McGale, P., McGrath, J., Mehta, S., Memish, Z. A., Mensah, G. A., Merriman, T. R.,  
431 Micha, R., Michaud, C., Mishra, V., Hanafiah, K. M., Mokdad, A. A., Morawska, L., Mozaffarian, D., Murphy, T.,  
432 Naghavi, M., Neal, B., Nelson, P. K., Nolla, J. M., Norman, R., Olives, C., Omer, S. B., Orchard, J., Osborne, R., Ostro,  
433 B., Page, A., Pandey, K. D., Parry, C. D. H., Passmore, E., Patra, J., Pearce, N., Pelizzari, P. M., Petzold, M., Phillips, M.  
434 R., Pope, D., Pope, C. A., Powles, J., Rao, M., Razavi, H., Rehfuess, E. A., Rehm, J. T., Ritz, B., Rivara, F. P., Roberts,  
435 T., Robinson, C., Rodriguez-Portales, J. A., Romieu, I., Room, R., Rosenfeld, L. C., Roy, A., Rushton, L., Salomon, J.  
436 A., Sampson, U., Sanchez-Riera, L., Sanman, E., Sapkota, A., Seedat, S., Shi, P., Shield, K., Shivakoti, R., Singh, G. M.,  
437 Sleet, D. A., Smith, E., Smith, K. R., Stapelberg, N. J. C., Steenland, K., Stöckl, H., Stovner, L. J., Straif, K., Straney, L.,  
438 Thurston, G. D., Tran, J. H., Van Dingenen, R., van Donkelaar, A., Veerman, J. L., Vijayakumar, L., Weintraub, R.,  
439 Weissman, M. M., White, R. A., Whiteford, H., Wiersma, S. T., Wilkinson, J. D., Williams, H. C., Williams, W., Wilson,  
440 N., Woolf, A. D., Yip, P., Zielinski, J. M., Lopez, A. D., Murray, C. J. L., and Ezzati, M.: A comparative risk assessment  
441 of burden of disease and injury attributable to 67 risk factors and risk factor clusters in 21 regions, 1990–2010: a  
442 systematic analysis for the Global Burden of Disease Study 2010, *Lancet.*, 380, 2224–2260,  
443 [https://doi.org/10.1016/S0140-6736\(12\)61766-8](https://doi.org/10.1016/S0140-6736(12)61766-8), 2012.
- 444 Liu, S., Liu, Z., Li, J., Wang, Y., Ma, Y., Sheng, L., Liu, H., Liang, F., Xin, G., and Wang, J.: Numerical simulation for the  
445 coupling effect of local atmospheric circulations over the area of Beijing, Tianjin and Hebei Province, *Sci. China Ser. D*  
446 *Earth Sci.*, 52, 382–392, <https://doi.org/10.1007/s11430-009-0030-2>, 2009.
- 447 Luo, M., Hou, X., Gu, Y., Lau, N.-C., and Yim, S. H.-L.: Trans-boundary air pollution in a city under various atmospheric  
448 conditions, *Sci. Total Environ.*, 618, 132–141, <https://doi.org/10.1016/j.scitotenv.2017.11.001>, 2018.
- 449 Luo, Y., Lu, D., Zhou, X., Li, W., and He, Q.: Characteristics of the spatial distribution and yearly variation of aerosol optical  
450 depth over China in last 30 years, *J. Geophys. Res.*, 106, 14501–14513, <https://doi.org/10.1029/2001JD900030>, 2001.
- 451 MEP: China National Ambient Air Quality Standards, MEP, Beijing, China, 2012.
- 452 Miao, Y., Liu, S., Zheng, Y., Wang, S., Chen, B., Zheng, H., and Zhao, J.: Numerical study of the effects of local atmospheric  
453 circulations on a pollution event over Beijing–Tianjin–Hebei, China, *J. Environ. Sci.*, 30, 9–20,  
454 <https://doi.org/10.1016/j.jes.2014.08.025>, 2015.
- 455 Ni, C., Li, G., and Xiong, X.: Analysis of a vortex precipitation event over Southwest China using AIRS and in situ  
456 measurements, *Adv. Atmos. Sci.*, 34, 559–570, <https://doi.org/10.1007/s00376-016-5262-4>, 2017.



- 457 Ning, G., Wang, S., Ma, M., Ni, C., Shang, Z., Wang, J., and Li, J.: Characteristics of air pollution in different zones of  
458 Sichuan Basin, China, *Sci. Total Environ.*, 612, 975-984, <https://doi.org/10.1016/j.scitotenv.2017.08.205>, 2018.
- 459 Peng, X., and Cheng, L.: A case numerical study on the evolution of the plateau-east-side low vortex and shear line. Part  
460 I: Analysis and diagnosis, *J. Lanzhou Univ. Nat. Sci.*, 28, 163-168,  
461 <https://doi.org/10.13885/j.issn.0455-2059.1992.02.029>, 1992.
- 462 Qu, Y., Han, Y., Wu, Y., Gao, P., and Wang, T.: Study of PBLH and Its Correlation with Particulate Matter from One-Year  
463 Observation over Nanjing, Southeast China, *Remote Sens.*, 9, 668, 2017.
- 464 Quan, J., Gao, Y., Zhang, Q., Tie, X., Cao, J., Han, S., Meng, J., Chen, P., and Zhao, D.: Evolution of planetary boundary  
465 layer under different weather conditions, and its impact on aerosol concentrations, *Particuology.*, 11, 34-40,  
466 <https://doi.org/10.1016/j.partic.2012.04.005>, 2013.
- 467 Shi, Y., Zhang, N., Gao, J., Li, X., and Cai, Y.: Effect of fireworks display on perchlorate in air aerosols during the Spring  
468 Festival, *Atmos. Environ.*, 45, 1323-1327, <https://doi.org/10.1016/j.atmosenv.2010.11.056>, 2011.
- 469 Slingo, J. M.: The Development and Verification of A Cloud Prediction Scheme For the Ecmwf Model, *Q. J. Roy. Meteor.*  
470 *Soc.*, 113, 899-927, <https://doi.org/10.1002/qj.49711347710>, 1987.
- 471 Tao, J., Cheng, T., Zhang, R., Cao, J., Zhu, L., Wang, Q., Luo, L., and Zhang, L.: Chemical composition of PM<sub>2.5</sub> at an  
472 urban site of Chengdu in southwestern China, *Adv. Atmos. Sci.*, 30, 1070-1084,  
473 <https://doi.org/10.1007/s00376-012-2168-7>, 2013a.
- 474 Tao, J., Zhang, L., Engling, G., Zhang, R., Yang, Y., Cao, J., Zhu, C., Wang, Q., and Luo, L.: Chemical composition of PM<sub>2.5</sub>  
475 in an urban environment in Chengdu, China: Importance of springtime dust storms and biomass burning, *Atmos. Res.*,  
476 122, 270-283, <https://doi.org/10.1016/j.atmosres.2012.11.004>, 2013b.
- 477 Tao, M., Chen, L., Su, L., and Tao, J.: Satellite observation of regional haze pollution over the North China Plain, *J. Geophys.*  
478 *Res.-Atmos.*, 117, n/a-n/a, 10.1029/2012JD017915, 2012.
- 479 Tao, M., Chen, L., Xiong, X., Zhang, M., Ma, P., Tao, J., and Wang, Z.: Formation process of the widespread extreme haze  
480 pollution over northern China in January 2013: Implications for regional air quality and climate, *Atmos. Environ.*, 98,  
481 417-425, <https://doi.org/10.1016/j.atmosenv.2014.09.026>, 2014.
- 482 Tian, P., Cao, X., Zhang, L., Sun, N., Sun, L., Logan, T., Shi, J., Wang, Y., Ji, Y., Lin, Y., Huang, Z., Zhou, T., Shi, Y., and  
483 Zhang, R.: Aerosol vertical distribution and optical properties over China from long-term satellite and ground-based  
484 remote sensing, *Atmos. Chem. Phys.*, 17, 2509-2523, <https://doi.org/10.5194/acp-17-2509-2017>, 2017.
- 485 Wang, Q.-W., and Tan, Z.-M.: Multi-scale topographic control of southwest vortex formation in Tibetan Plateau region in an  
486 idealized simulation, *J. Geophys. Res.-Atmos.*, 119, 5143-5156, <https://doi.org/10.1002/2014JD021898>, 2014.
- 487 Wang, T., Nie, W., Gao, J., Xue, L. K., Gao, X. M., Wang, X. F., Qiu, J., Poon, C. N., Meinardi, S., Blake, D., Wang, S. L.,  
488 Ding, A. J., Chai, F. H., Zhang, Q. Z., and Wang, W. X.: Air quality during the 2008 Beijing Olympics: secondary  
489 pollutants and regional impact, *Atmos. Chem. Phys.*, 10, 7603-7615, <https://doi.org/10.5194/acp-10-7603-2010>, 2010.
- 490 Wang, Y., Zhuang, G., Xu, C., and An, Z.: The air pollution caused by the burning of fireworks during the lantern festival in  
491 Beijing, *Atmos. Environ.*, 41, 417-431, <https://doi.org/10.1016/j.atmosenv.2006.07.043>, 2007.



- 492 Wang, Y., Hao, J., McElroy, M. B., Munger, J. W., Ma, H., Chen, D., and Nielsen, C. P.: Ozone air quality during the 2008  
493 Beijing Olympics: effectiveness of emission restrictions, *Atmos. Chem. Phys.*, 9, 5237-5251,  
494 <https://doi.org/10.5194/acp-9-5237-2009>, 2009.
- 495 Wang, Y., Yao, L., Wang, L., Liu, Z., Ji, D., Tang, G., Zhang, J., Sun, Y., Hu, B., and Xin, J.: Mechanism for the formation of  
496 the January 2013 heavy haze pollution episode over central and eastern China, *Sci. China Earth. Sci.*, 57, 14-25,  
497 <https://doi.org/10.1007/s11430-013-4773-4>, 2014.
- 498 Wei, P., Cheng, S., Li, J., and Su, F.: Impact of boundary-layer anticyclonic weather system on regional air quality, *Atmos.*  
499 *Environ.*, 45, 2453-2463, <https://doi.org/10.1016/j.atmosenv.2011.01.045>, 2011.
- 500 Whiteman, C. D., Hoch, S. W., Horel, J. D., and Charland, A.: Relationship between particulate air pollution and  
501 meteorological variables in Utah's Salt Lake Valley, *Atmos. Environ.*, 94, 742-753,  
502 <https://doi.org/10.1016/j.atmosenv.2014.06.012>, 2014.
- 503 Wu, P., Ding, Y., and Liu, Y.: Atmospheric circulation and dynamic mechanism for persistent haze events in the  
504 Beijing–Tianjin–Hebei region, *Adv. Atmos. Sci.*, 34, 429-440, <https://doi.org/10.1007/s00376-016-6158-z>, 2017.
- 505 Yang, L., Wu, Y., Davis, J. M., and Hao, J.: Estimating the effects of meteorology on PM<sub>2.5</sub> reduction during the 2008  
506 Summer Olympic Games in Beijing, China, *Front Environ Sci Eng.*, 5, 331, <https://doi.org/10.1007/s11783-011-0307-5>,  
507 2011.
- 508 Ye, X., Song, Y., Cai, X., and Zhang, H.: Study on the synoptic flow patterns and boundary layer process of the severe haze  
509 events over the North China Plain in January 2013, *Atmos. Environ.*, 124, 129-145,  
510 <https://doi.org/10.1016/j.atmosenv.2015.06.011>, 2016.
- 511 Yu, S., Gao, W., Xiao, D., and Peng, J.: Observational facts regarding the joint activities of the southwest vortex and plateau  
512 vortex after its departure from the Tibetan Plateau, *Adv. Atmos. Sci.*, 33, 34-46,  
513 <https://doi.org/10.1007/s00376-015-5039-1>, 2016.
- 514 Zeng, S., and Zhang, Y.: The Effect of Meteorological Elements on Continuing Heavy Air Pollution: A Case Study in the  
515 Chengdu Area during the 2014 Spring Festival, *Atmosphere.*, 8, 71, <https://doi.org/10.3390/atmos8040071>, 2017.
- 516 Zhang, J., Luo, B., Zhang, J., Ouyang, F., Song, H., Liu, P., Cao, P., Schäfer, K., Wang, S., Huang, X., and Lin, Y.: Analysis  
517 of the characteristics of single atmospheric particles in Chengdu using single particle mass spectrometry, *Atmos.*  
518 *Environ.*, 157, 91-100, <https://doi.org/10.1016/j.atmosenv.2017.03.012>, 2017.
- 519 Zhang, J. P., Zhu, T., Zhang, Q. H., Li, C. C., Shu, H. L., Ying, Y., Dai, Z. P., Wang, X., Liu, X. Y., Liang, A. M., Shen, H. X.,  
520 and Yi, B. Q.: The impact of circulation patterns on regional transport pathways and air quality over Beijing and its  
521 surroundings, *Atmos. Chem. Phys.*, 12, 5031-5053, <https://doi.org/10.5194/acp-12-5031-2012>, 2012a.
- 522 Zhang, S.-t., and Niu, S.-j.: HAZE-TO-FOG TRANSFORMATION DURING A LONG LASTING, LOW VISIBILITY  
523 EPISODE IN NANJING, *J. Trop. Meteorol.*, 22, 67-77, <https://doi.org/10.16555/j.1006-8775.2016.S1.007>, 2016.
- 524 Zhang, X. Y., Wang, Y. Q., Niu, T., Zhang, X. C., Gong, S. L., Zhang, Y. M., and Sun, J. Y.: Atmospheric aerosol  
525 compositions in China: spatial/temporal variability, chemical signature, regional haze distribution and comparisons with  
526 global aerosols, *Atmos. Chem. Phys.*, 12, 779-799, <https://doi.org/10.5194/acp-12-779-2012>, 2012b.



527 Zhang, Z., Zhang, X., Gong, D., Kim, S. J., Mao, R., and Zhao, X.: Possible influence of atmospheric circulations on winter  
528 haze pollution in the Beijing–Tianjin–Hebei region, northern China, Atmos. Chem. Phys., 16, 561-571,  
529 <https://doi.org/10.5194/acp-16-561-2016>, 2016.



530

**Table 1.** Overview of the eight heavy air pollution events affected by dry low-pressure systems.

Event	Most polluted city	Heavy air pollution event		Most polluted day			End date of heavy air pollution event			Other cities with heavy air pollution
		Start and end dates of air pollution event	PM <sub>10</sub> concentration range in this period (µg m <sup>-3</sup> )	Date	PM <sub>10</sub> concentration (µg m <sup>-3</sup> )	Visibility (m)	Date	PM <sub>10</sub> concentration (µg m <sup>-3</sup> )	Visibility (m)	
1	Mianyang	13–14 Jan 2006	284–442	13 Jan 2006	442	800	15 Jan 2006	166	12000	Chengdu
2	Chengdu	29 Jan 2006	407	29 Jan 2006	407	<50	30 Jan 2006	190	11000	None
3	Chengdu	19–23 Dec 2006	348–385	23 Dec 2006	385	1500	24 Dec 2006	246	11000	None
4	Chengdu	21–24 Dec 2007	260–529	23 Dec 2007	529	800	25 Dec 2007	174	3000	Mianyang
5	Chengdu	18–20 Jan 2009	264–381	19 Jan 2009	381	<50	21 Jan 2009	220	11000	Mianyang
6	Chengdu	3 Feb 2011	403	3 Feb 2011	403	2000	4 Feb 2011	190	11000	None
7	Chengdu	22–31 Jan 2014	282–562	31 Jan 2014	562	<500	1 Feb 2014	207	2500	Deyang
8	Chengdu	1–6 Jan 2017	294–480	5 Jan 2017	480	100	7 Jan 2017	118	11000	Deyang

531

532

**Table 2.** Relative vorticity at 700 hPa during the periods of deteriorating and improving air quality in the eight heavy air pollution events.

534

535

Event	Deteriorating air quality		Improving air quality	
	Time (BST)	Relative vorticity (1×10 <sup>-5</sup> s <sup>-1</sup> )	Time (BST)	Relative vorticity (1×10 <sup>-5</sup> s <sup>-1</sup> )
1	02:00 on 13 Jan 2006	2.58	20:00 on 13 Jan 2006	-0.94
2	02:00 on 29 Jan 2006	4.15	08:00 on 30 Jan 2006	-3.36
3	20:00 on 22 Dec 2006	4.64	14:00 on 23 Dec 2006	-1.09
4	14:00 on 22 Dec 2007	0.59	14:00 on 23 Dec 2007	-0.82
5	02:00 on 19 Jan 2009	1.75	08:00 on 19 Jan 2009	-2.48
6	02:00 on 3 Feb 2011	2.96	14:00 on 3 Feb 2011	3.16
7	02:00 on 31 Jan 2014	9.12	02:00 on 1 Feb 2014	5.49
8	20:00 on 4 Jan 2017	6.49	08:00 on 5 Jan 2017	-5.74

536

537



538 **Table 3.** Height of the atmospheric boundary layer (BLH), lower tropospheric stability (LTS), and mean wind speed  
539 (MWS) in the lower troposphere during periods of deteriorating and improving air quality in the eight heavy air  
540 pollution events.  
541

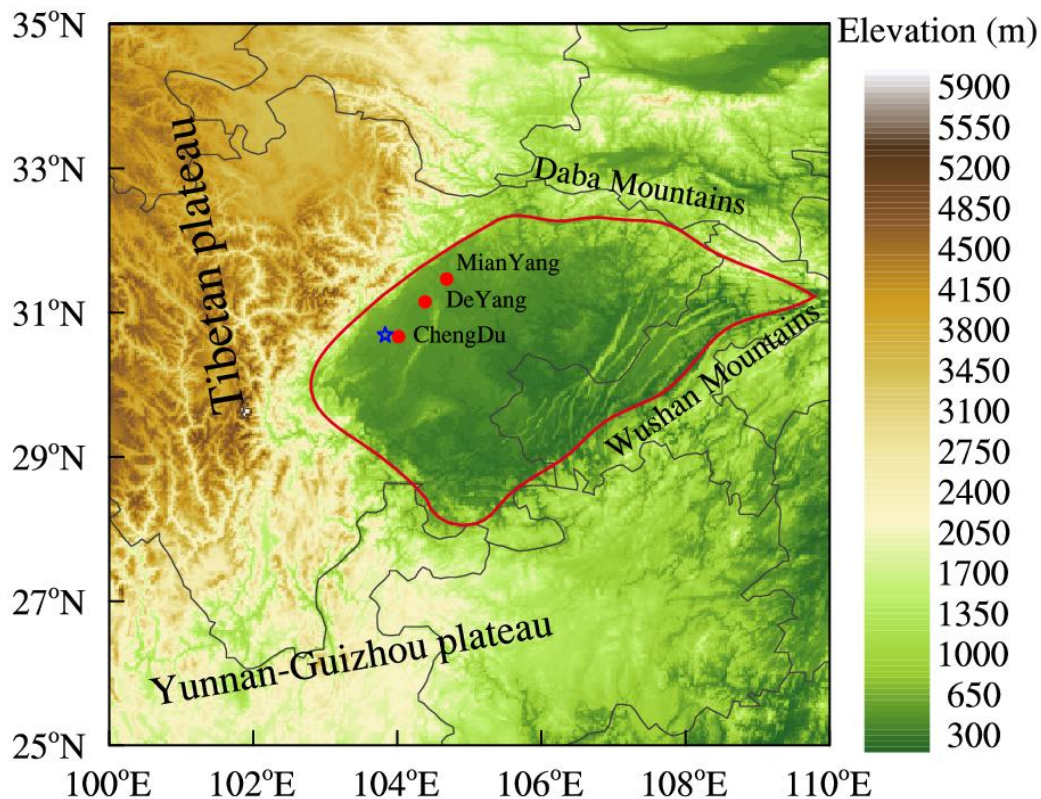
Event	Deteriorating air quality			Differences between periods of improving and deteriorating air quality		
	BLH (m)	LTS (K)	MWS ( $\text{m s}^{-1}$ )	BLH (m)	LTS (K)	WMS ( $\text{m s}^{-1}$ )
1	278.16	23.13	2.86	144.75	-11.23	0.41
2	375.42	29.45	4.12	139.08	-10.2	1.93
3	279.50	18.54	2.99	-16.45	-5.61	0.34
4	282.61	18.58	1.91	-39.62	-7.23	1.04
5	251.53	19.63	3.11	51.17	-7.88	0.85
6	282.16	25.80	4.22	-16.87	0.55	1.91
7	232.57	25.95	4.21	30.77	-1.97	-1.07
8	266.23	18.88	2.59	107.57	-8.4	0.27

542

543



544



545

546

547

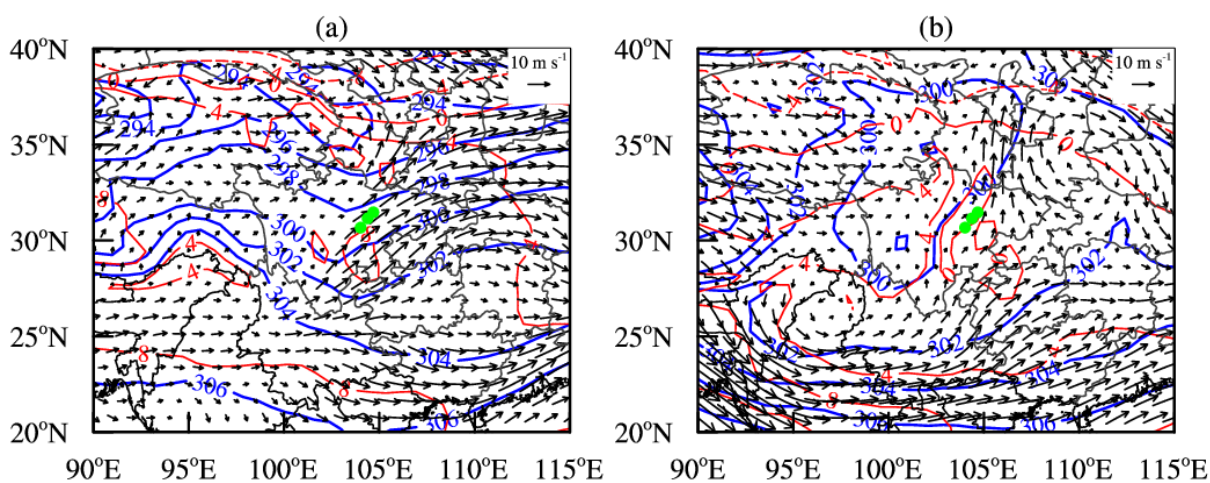
548

549

**Fig. 1** Topographic map (shading, units: m) of the Sichuan Basin (delineated in red) and surrounding areas showing the location of the cities of Chengdu, Deyang, and Mianyang (red dots). The Wenjiang station is marked with blue five-pointed stars. For interpretation of the colors, see web version of this article.



550



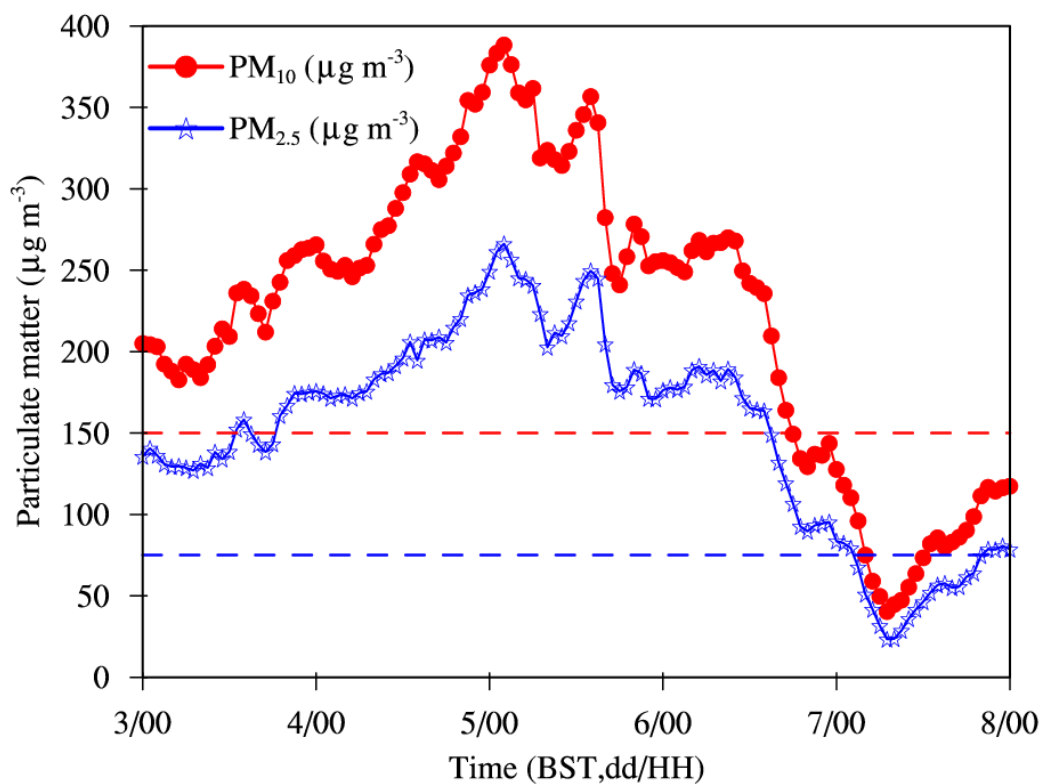
551

552 **Fig. 2** Weather maps at 700 hPa based on ERA-Interim daily data showing (a) a trough and (b) a low vortex. The blue  
553 lines are isopleths of geopotential height, the red lines are isotherms and the black arrows are wind vectors. The green  
554 dots show the location of the urban agglomeration.

555



556



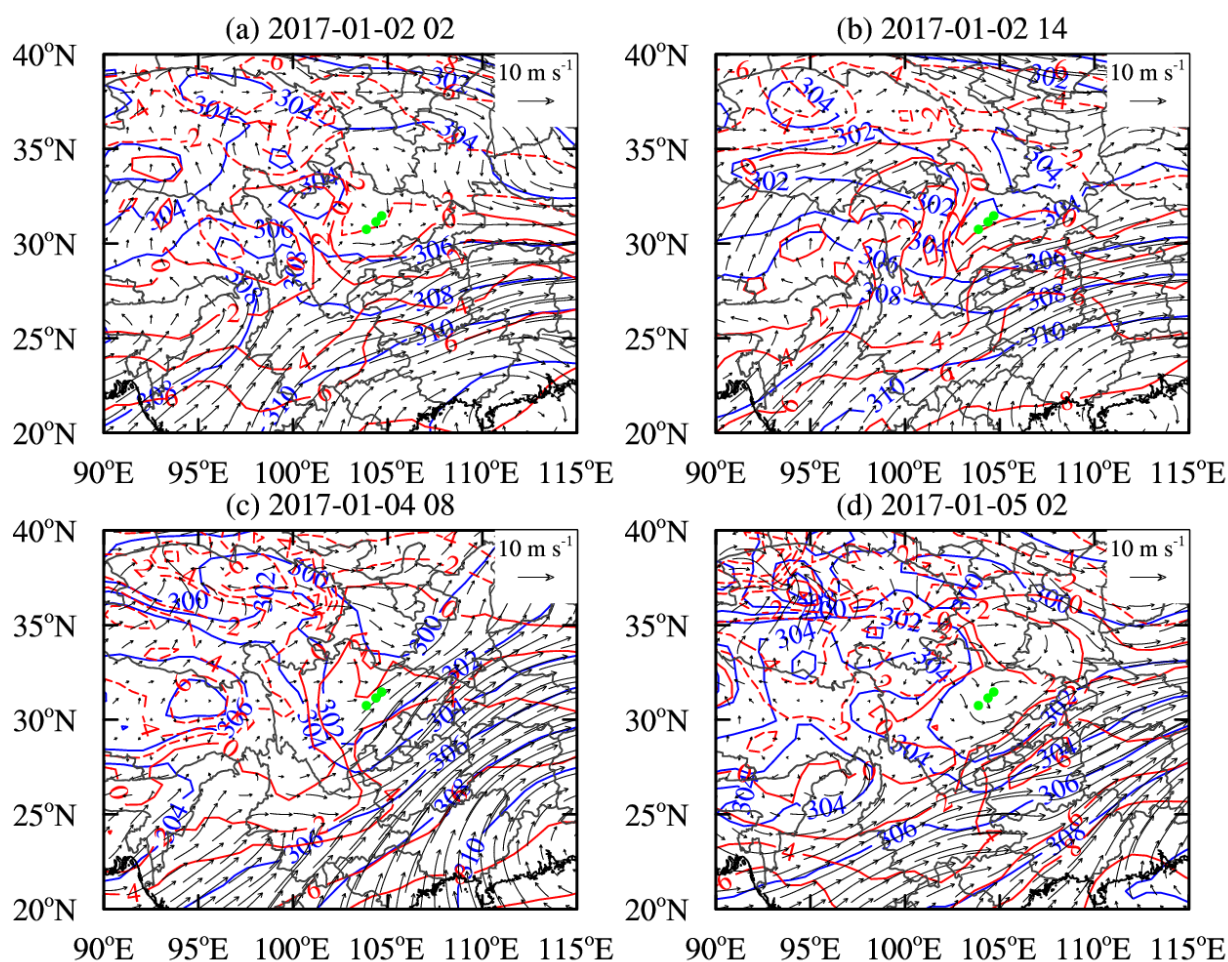
557

558 **Fig. 3** Average hourly concentrations of surface PM<sub>10</sub> (red solid line) and PM<sub>2.5</sub> (blue solid line) in the urban  
559 agglomeration from 00:00 BST on 3 January 2017 to 00:00 BST on 8 January 2017 during event 8. The dashed red  
560 line represents Grade II standard of PM<sub>10</sub> daily concentration ( $150 \mu\text{g m}^{-3}$ ), the dashed blue line represents Grade II  
561 standard of PM<sub>2.5</sub> daily concentration ( $75 \mu\text{g m}^{-3}$ ).

562



563



564

565

566

567

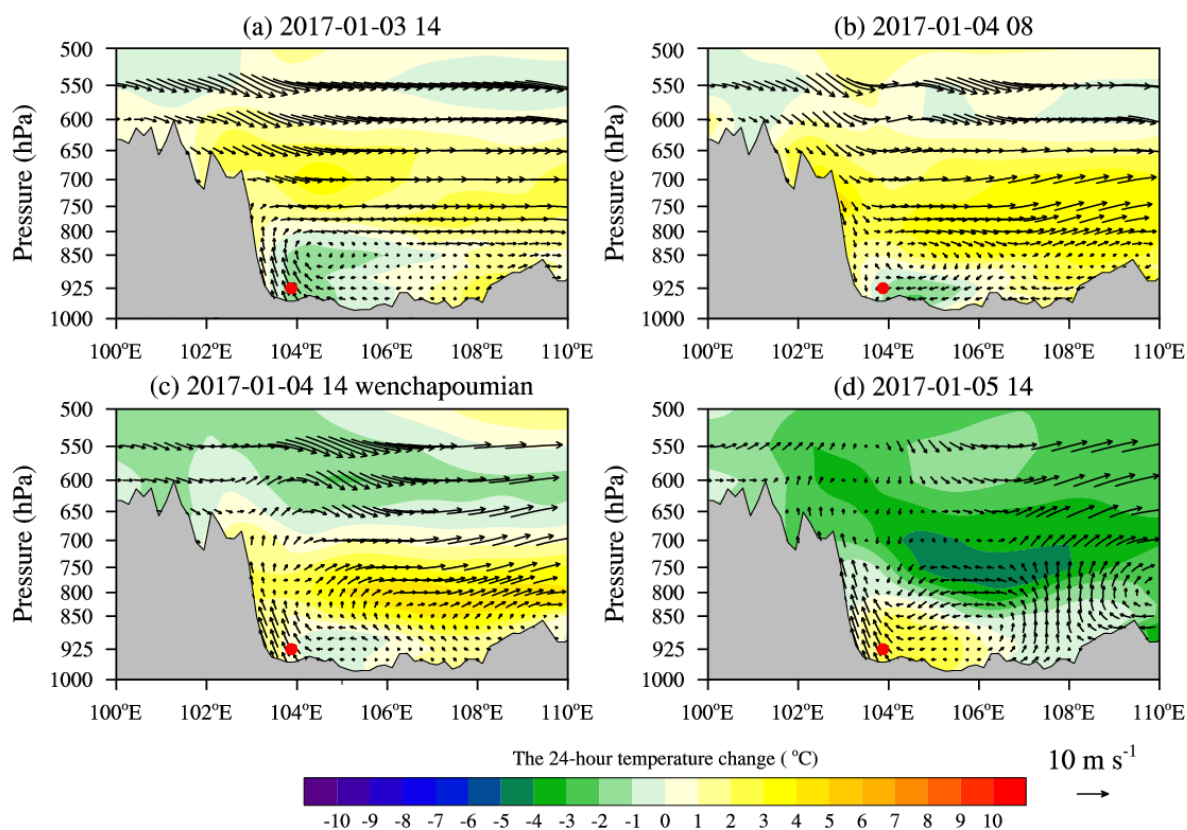
568

569

**Fig. 4** Weather maps at 700 hPa for event 8 at (a) 02:00 BST on 2 January 2017, (b) 14:00 BST on 2 January 2017, (c) 08:00 BST on 4 January 2017 and (d) 02:00 BST on 5 January 2017. The blue lines are isopleths of geopotential height, the red lines are isotherms and the black arrows are wind vectors. The green dots show the location of the urban agglomeration.



570



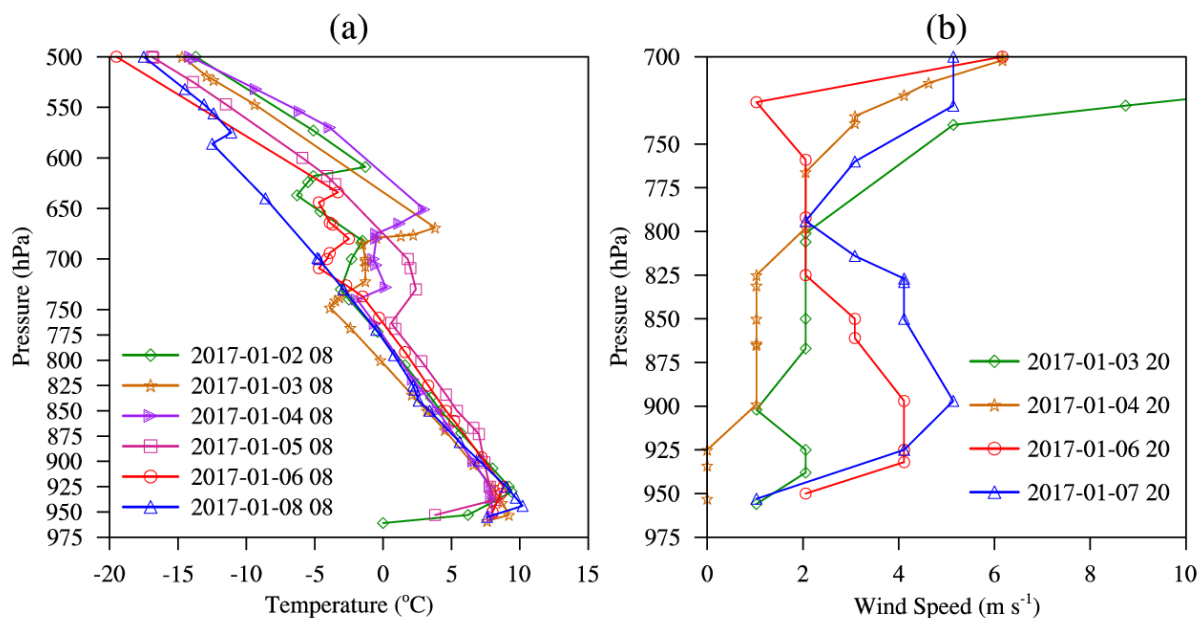
571

572 **Fig. 5** West-to-east vertical cross-sections of 24-hour temperature change (shading, units: °C) and wind vectors  
573 (synthesized by u and w) through the most polluted area (30.75 °N) during event 8 at (a) 14:00 BST on 3 January 2017,  
574 (b) 08:00 BST on 4 January 2017, (c) 14:00 BST on 4 January 2017 and (d) 14:00 BST on 5 January 2017 during  
575 event 8. Note that the vertical velocity is multiplied by 100 when plotting the wind vectors. The most polluted area is  
576 marked by red solid dots. The gray shading represents the terrain.

577



578



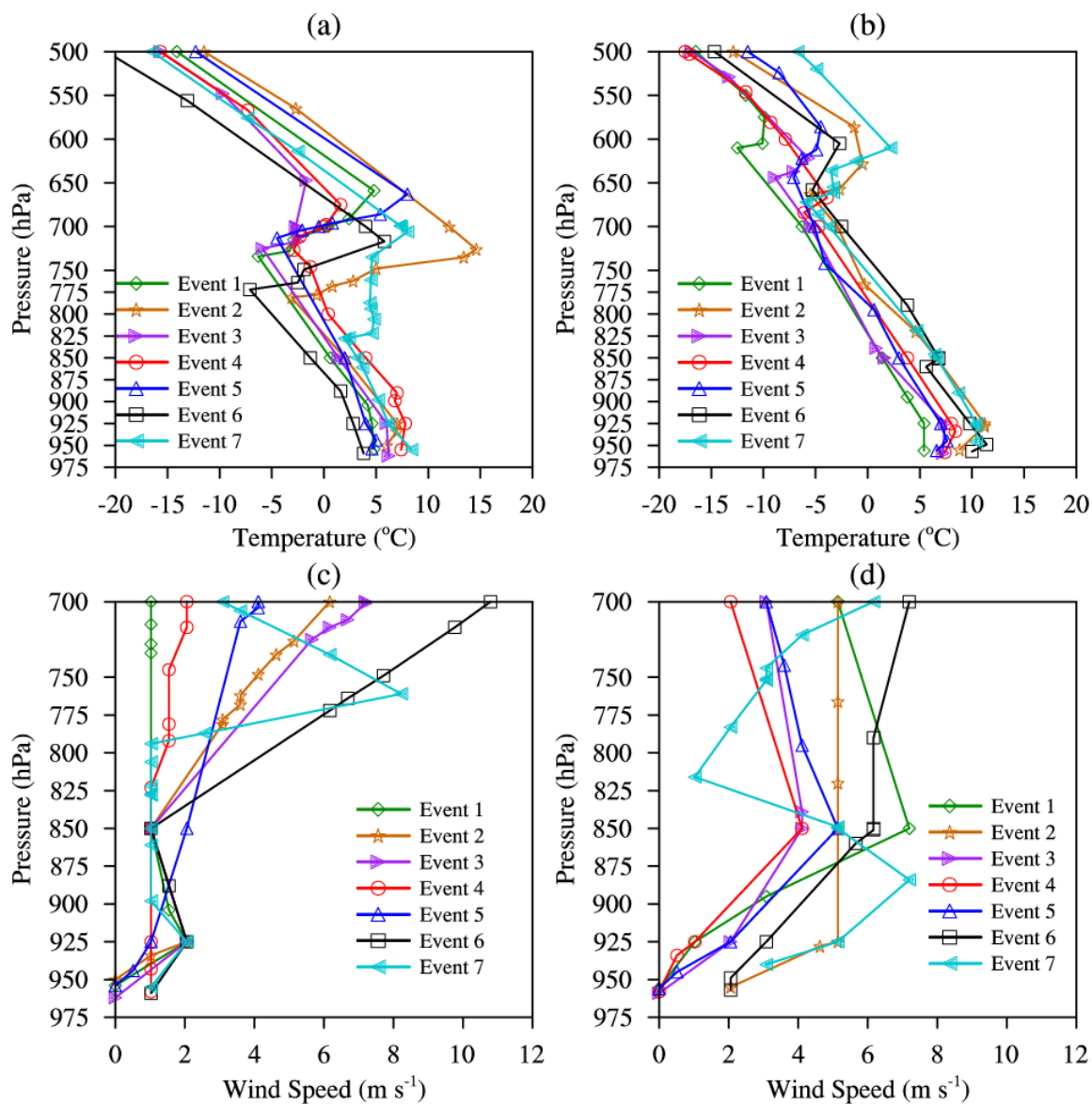
579

580 **Fig. 6** Vertical profiles of (a) temperature and (b) horizontal wind speed at Wenjiang station (30.75 °N, 103.875 °E,  
581 see **Fig. 1**) measured by radiosonde during event 8.

582



583



584

585

586

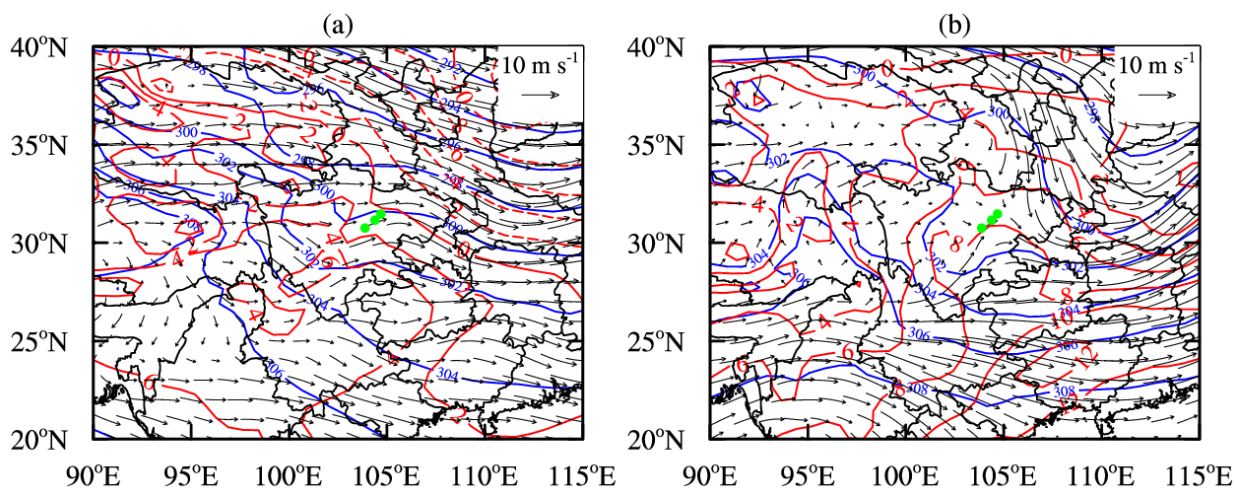
587

588

**Fig. 7** Vertical profiles of (a) temperature and (c) horizontal wind speed in the urban agglomeration during periods controlled by the low-pressure system. Vertical profiles of (b) temperature and (d) horizontal wind speed after the low-pressure system had transited across the urban agglomeration for seven heavy air pollution events (events 1–7).



589



590

591

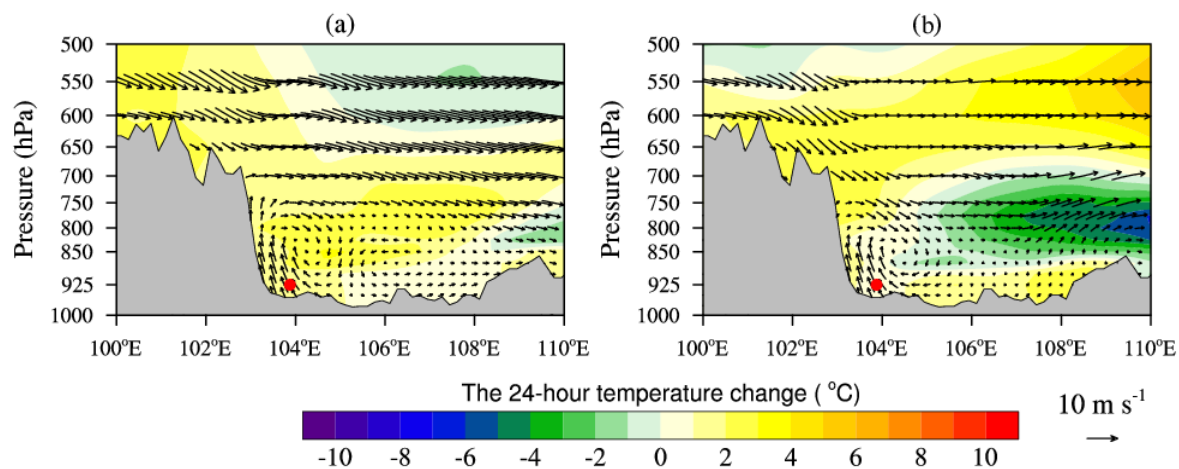
592

593

**Fig. 8** Weather maps at 700 hPa during periods of improving air quality (a) for event 6 and (b) for event 7. The blue lines are isopleths of geopotential height, the red lines are isotherms and the black arrows are wind vectors. The green dots show the location of the urban agglomeration.



594



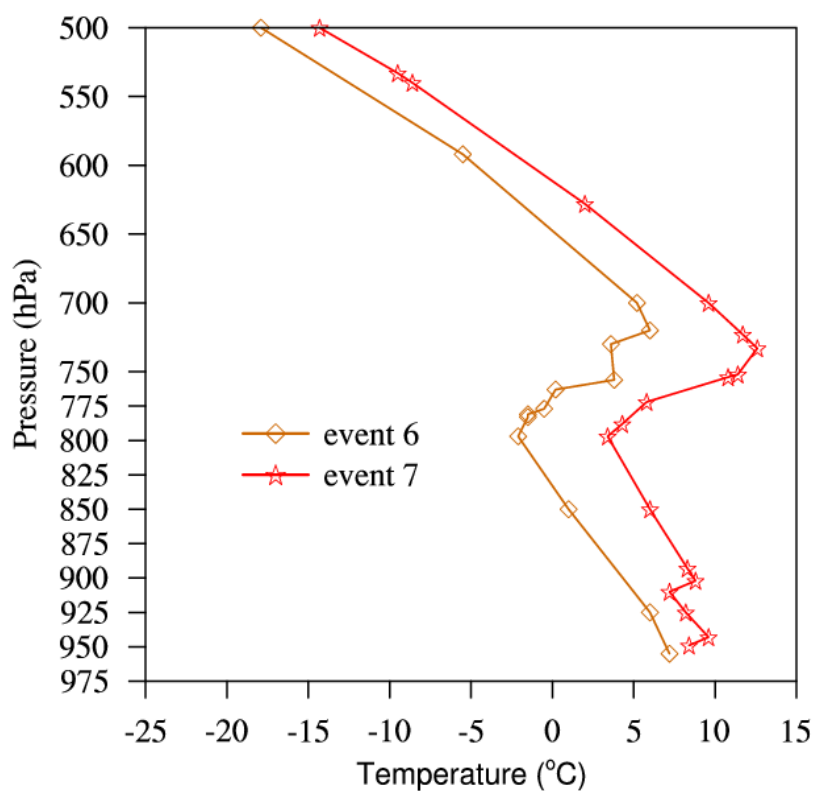
595

596 **Fig. 9** West-to-east vertical cross-sections of 24-hour temperature change (shading, units: °C) and wind vectors  
597 (synthesized by u and w) through the most polluted area (30.75 °N) during the periods of improving air quality (a) for  
598 event 6 and (b) for event 7. Note that the vertical velocity is multiplied by 100 when plotting the wind vectors. The  
599 most polluted area is marked by red solid dots. The gray shading represents the terrain.

600



601



602

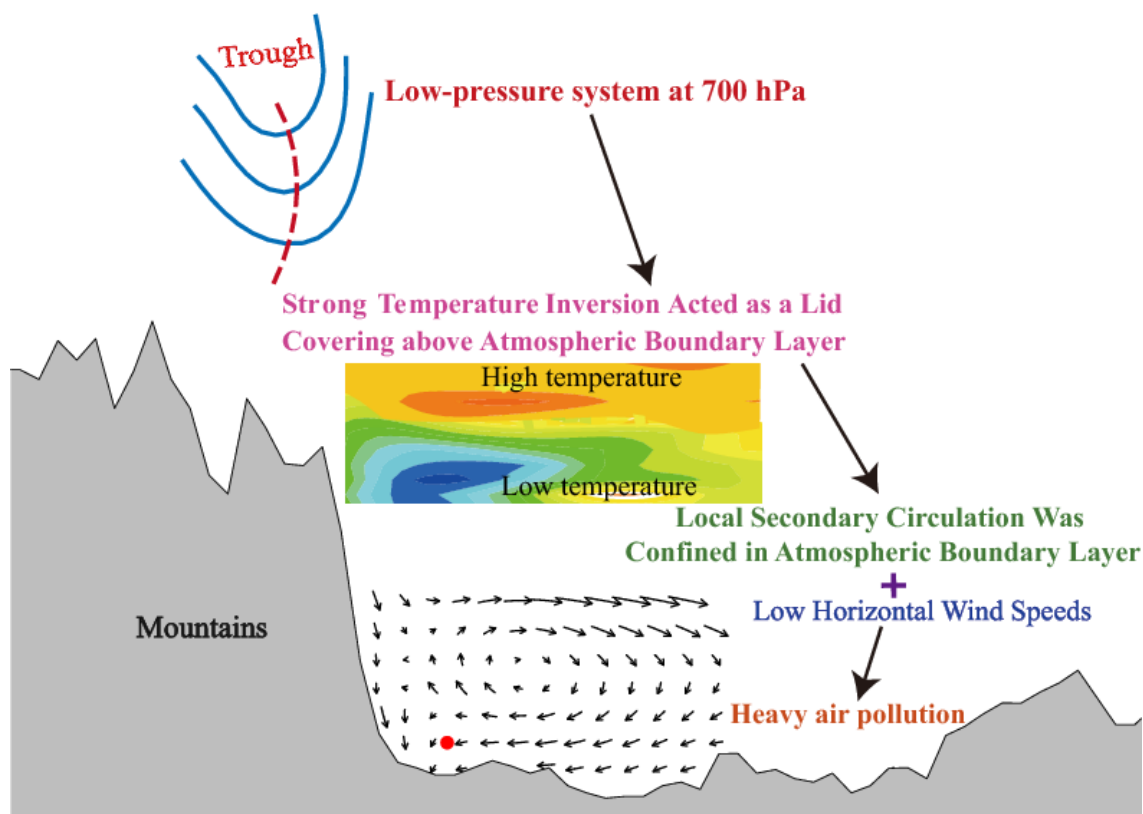
603 **Fig. 10** Vertical profiles of temperature at Wenjiang station (30.75 °N, 103.875 °E) measured by radiosonde during  
604 periods of improving air quality for event 6 and 7.

605

606



607



608

609 **Fig. 11** Schematic diagram of the mechanism of influence of a dry low-pressure system on winter heavy air pollution  
610 events in the urban agglomeration.

611

612